Progress in top-quark pair production cross section calculations and impact on PDFs

Marco Guzzi

Kennesaw State University

with

A. Ablat, S. Dulat, T.-J. Hou, I. Sitiwaldi, K. Xie, C.-P. Yuan,

and with N. Kidonakis, and A. Tonero

LHCP2024, Tue June 5, 2024, Northeastern University, Boston, MA

Main goals and motivations

$t\bar{t}$ production at the LHC: clean probe for PDFs at intermediate and large x (where it complements jet prod.) PDFs currently poorly constrained at large x.

➢Toward the next (CT2X) CTEQ-PDFs release. Efforts are being put into:

1. Selecting sensitive data from recent high-precision measurements at the LHC
2. Understand current PDF uncertainties (tolerance, methodology, functional forms,…)
3. State-of-the-art calculations

This talk:

➢eligible $t\bar{t}$ production 1D abs. diff. Xsec measurements at the LHC 13 TeV and their impact on the gluon at large x from an optimal baseline selection in NNLO global fits
(Ablat, MG, Xie, et al. 2307.11153, PRD 2024)

➢Explore the impact of aN^3LO QCD corrections + NLO EW on $t\bar{t}$ observables
(Kidonakis, MG, Tonero, 2306.06166, PRD 2023)

PDF Kinematics in the $\boldsymbol{Q}$-$\boldsymbol{x}$ plane

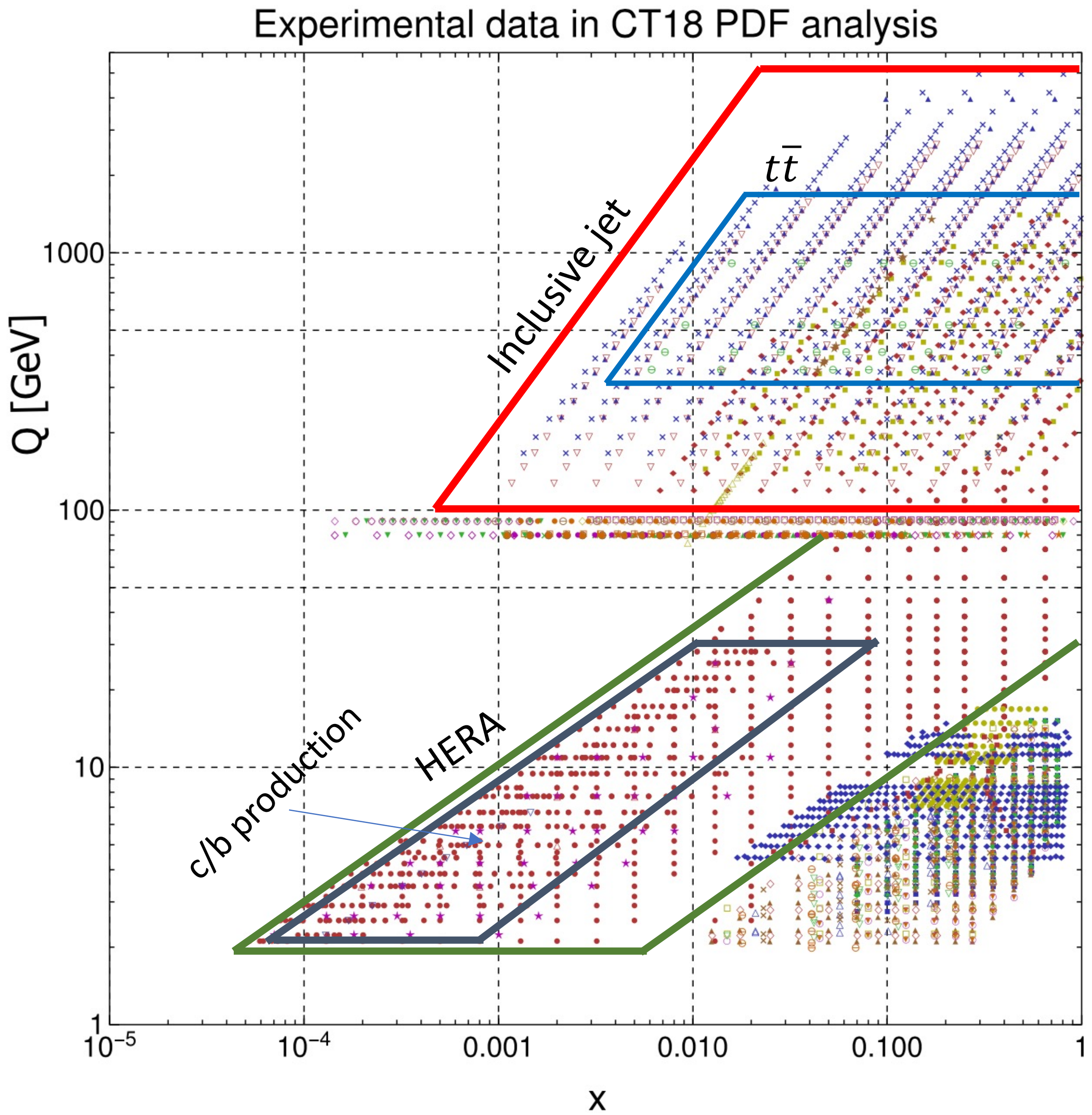

Top-quark pair production @LHC can already probe the gluon PDF at $x \gtrsim 0.01$ ➡ $x_{1,2} \approx \frac{\sqrt{p_T^2 + m_Q^2}}{\sqrt{S}} e^{\pm y}$

Correlation plots with ePump

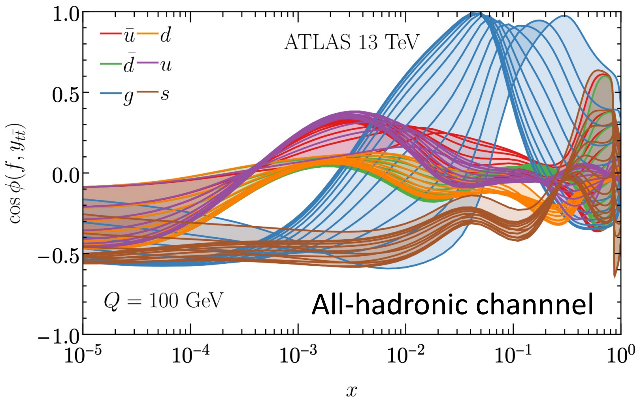

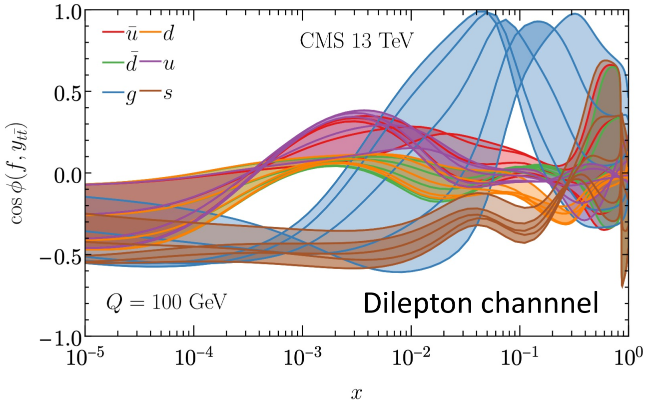

Jet and $t\bar{t}$ complement each other in the kinematic plane. They impact the gluon PDF at large x. Important to disentangle the effect due to jet production and top-quark data.

$t\bar{t}$ and jet data in CT18

Top-quark
1511.04716 ATLAS 8 TeV ttb ptT diff. distributions
1511.04716 ATLAS 8 TeV ttb mtt diff. distributions
1703.01630 CMS 8 TeV ttb (pT , yt) 2d diff. distrib.

Jet production
1406.0324 CMS incl. jet at 7 TeV with R=0.7
1410.8857 ATLAS incl. jet at 7 TeV with R=0.6
1609.05331 CMS incl. jet at 8 TeV with R=0.7

Constraints from 8 TeV $t\bar{t}$ production data in CT18

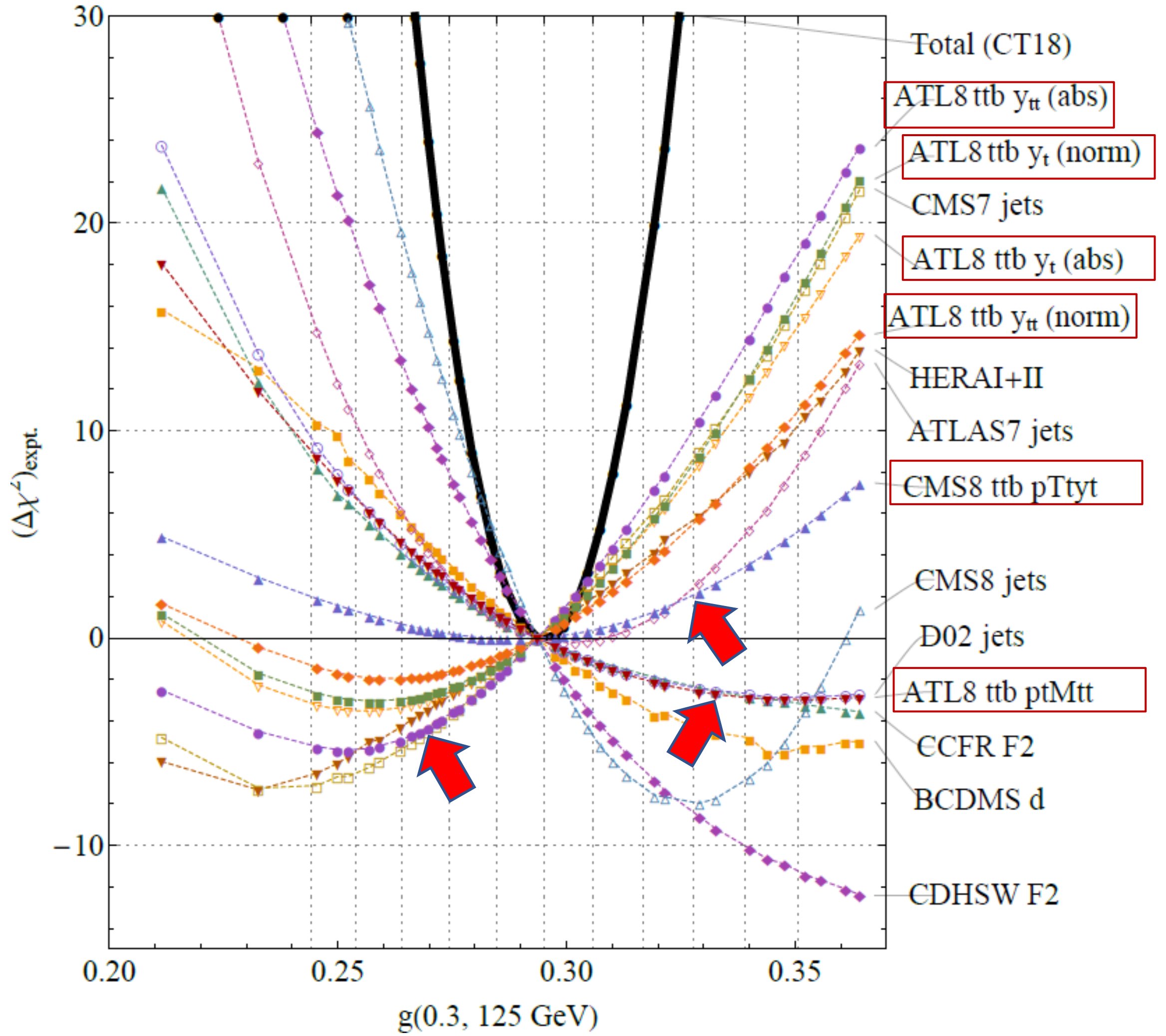

Figure by P. Nadolsky

Realistic PDF error estimates account for:

- multiple PDF functional forms
- disagreements between measurements

mild impact from $t\bar{t}$ data

In the figure: Pulls on the gluon from ATLAS8 $y_{t\bar{t}}$ and y_t distributions (absolute or normalized) agree with HERA DIS, oppose ATLAS8 $\mathrm{d}^2\sigma/(dp_{T,t}dm_{t\bar{t}})$ and CMS8 $\mathrm{d}^2\sigma/(dp_{T,t}dy_{t,ave})$

Impact of LHC 13 TeV $t\bar{t}$ production on CTEQ PDFs

CT2X ⊃ CT18 + new optimal combination of top-quark pair production @LHC13 TeV from:

- ATLAS all hadronic, JHEP 01 (2021) 033, arXiv:2006.09274
- ATLAS lepton + jets, EPJC 79 (2019) 1028, arXiv:1908.07305
- CMS dilepton, JHEP 1902 (2019) 149, arXiv:1811.06625
- CMS lepton + jets, PRD 104 092013 (2021), arXiv:2108.02803

(Ablat, MG, Xie, et al. 2307.11153, PRD 2024)

Correlated Systematic Uncertainties: **ATLAS -> nuisance parameters**
CMS -> Covariance matrix representation
(we converted to nuisance param.)

When statistical correlations not provided → data added one at a time on top of the CT18 baseline

We studied the impact on PDFs due to several factors such as:

- μ_F and μ_R scale dependence
- different binning for the same distribution
- statistical correlations

Exp	Obs	$N_{\rm pt}$	ePump H_T	ePump $H_T/2$	ePump $H_T/4$	Global fit $H_T/2$	Global fit $H_T/4$
ATL13had	$m_{t\bar{t}}$	9	1.75	1.57	1.60	1.53	1.47
	$H_T^{t\bar{t}}$	11	1.98	1.77	1.59	1.50	1.74
	$y_{t\bar{t}}$	12	1.28	1.15	0.94	1.05	1.07
	p_{T,t_1}	10	1.30	1.19	1.12	1.20	1.33
	p_{T,t_2}	8	1.13	0.84	1.05	0.84	1.59
CMS13ll	$m_{t\bar{t}}$	7	3.46	3.07	3.14	3.12	3.23
	$y_{t\bar{t}}$	10	1.66	0.97	0.68	0.94	0.67
	$p_{T,t}$	6	3.60	3.70	3.68	3.56	3.05
	y_t	10	1.33	0.94	0.87	1.00	0.69
CMS13lj	$m_{t\bar{t}}$	15	1.49	1.38	1.81	1.20	1.67
	$y_{t\bar{t}}$	10	6.47	6.24	6.42	6.01	5.88
ATL13lj	CMS bins						
	$m_{t\bar{t}}$	7	2.40	1.17	0.68	0.83	0.66
	$y_{t\bar{t}}$	10	0.91	0.69	0.62	0.74	0.75
	$p_{T,t}$	6	2.34	2.01	2.47	1.35	1.43
	y_t	10	1.30	1.07	1.10	1.16	0.68
	ATLAS bins without statistical correlation (NSC)						
	$m_{t\bar{t}}$	9	1.55	1.12	0.94	1.27	0.92
	$y_{t\bar{t}}$	7	0.91	0.74	0.80	0.76	0.90
	$y_{t\bar{t}}^B$	9	1.40	1.27	1.53	0.85	0.93
	$H_T^{t\bar{t}}$	9	1.35	0.91	0.93	0.81	0.80
	$m_{t\bar{t}} + y_{t\bar{t}} + y_{t\bar{t}}^B + H_T^{t\bar{t}}$	34	1.87	1.28	1.46	0.93	1.06
	ATLAS bins with statistical correlations (WSC)						
	$m_{t\bar{t}}$	9	1.68	1.35	0.98	1.29	0.96
	$y_{t\bar{t}}$	7	0.88	0.75	0.92	0.75	0.92
	$y_{t\bar{t}}^B$	9	1.06	0.87	1.01	0.86	0.99
	$H_T^{t\bar{t}}$	9	1.40	0.85	0.85	0.86	0.86
	$m_{t\bar{t}} + y_{t\bar{t}} + y_{t\bar{t}}^B + H_T^{t\bar{t}}$	34	3.10	1.61	1.32	1.59	1.32

Impact of new high-precision LHC 13 TeV $t\bar{t}$ data on the gluon PDF

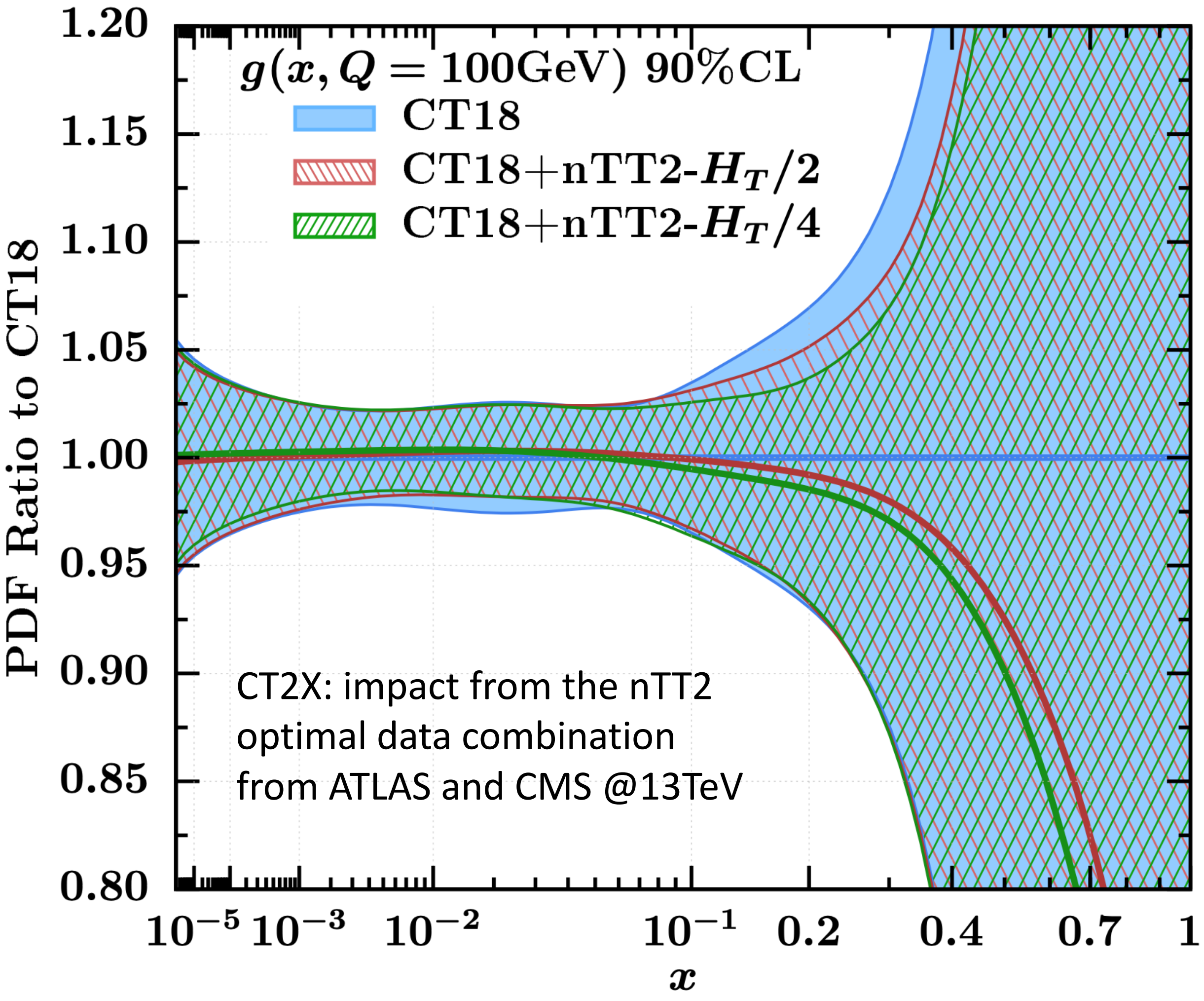

(Ablat, MG, Xie, Dulat, Hou, Sitiwaldi, Yuan, **PRD109 2024**; arXiv:2307.11153)

Theory predictions:
- MATRIX (Catani, Devoto, et al. PRD 2019, JHEP 2019)
- FastNNLO (Czakon, Mitov, 1704.08551; Czakon, Fiedler, et al., JHEP2016)

Blue band: CT18NNLO 90% C.L.
Hatched bands: CT18 + new top-quark data
Green: $\mu_R = \mu_F = H_T/2$
Red: $\mu_R = \mu_F = H_T/4$

Differences related to different scale choices are well within the CT18 PDF error band.

nTT2 baseline consists of 1D abs ttbar Xsec from:
- ATLAS all hadronic, ytt
- ATLAS lepton + jets, {ytt, Mtt, yBtt, HTtt} stat. comb.
- CMS dilepton, ytt
- CMS lepton + jets, Mtt

NNLO theory predictions: setup

- CMS (dilepton ch): FastNLO grids for the NNLO theory– (Czakon et al. 1704.08551)
- ATLAS: bin-by-bin NNLO/NLO K-factors generated by MATRIX (Catani, Devoto, et al. PRD2019; JHEP2019)

The NLO QCD calculation is obtained using our in-house APPLGrid fast tables (Carli et al. EPJC 2010) for the public MCFM calculation (Campbell, Ellis JPG 2015)

- m_t(pole) = 172.5 GeV
- Fact/Ren scale choice:

m_{tt}, $p_{T,tt}$, y_{tt}, y_t use: $H_T/4$ and $H_T/2$; $p_{T,t}$, use M_T; $p_{T,t\ avg}$ use $M_T/2$ (Czakon et al. JHEP 2017)

$$\mu_F = \mu_R = H_T/4 = \left(\sqrt{m_t^2 + p_{T,t}^2} + \sqrt{m_t^2 + p_{T,\bar{t}}^2}\right)/4 \qquad \mu_{F,R} = M_T^t/2 = \sqrt{m_t^2 + p_T^2}/2$$

- EW corrections considered: negligible impact on our fits.

Interplay between $t\bar{t}$ and QCD jets

- CT18mTop = CT18 without all $t\bar{t}$ 8 TeV and 13 TeV
- CT18mJet = CT18 without all jet data
- CT18mJet+nTT1-HT/2(4) = CT18 without all jet data, but with $t\bar{t}$ 13 TeV (HT/2(4) central scale)
- CT18mTop+nTT1-HT/2(4) = CT18 without all $t\bar{t}$ 8 TeV, but with $t\bar{t}$ 13 TeV (HT/2(4) central scale)

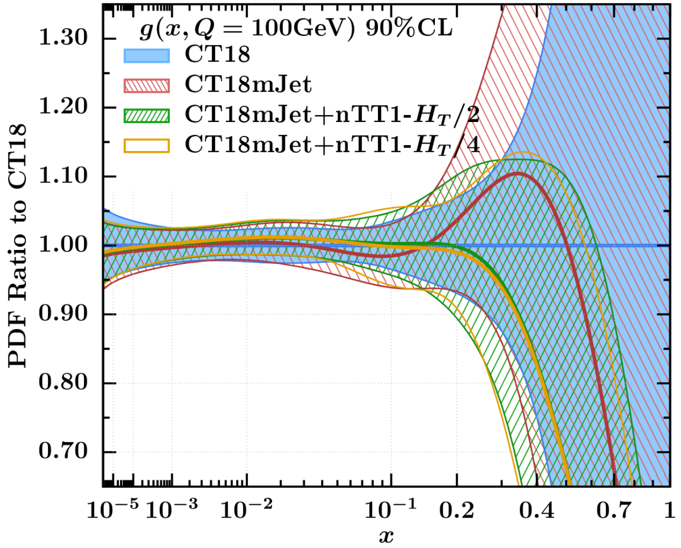

Global fit without jet data vs CT18NNLO

Global fit without $t\bar{t}$ data vs CT18NNLO

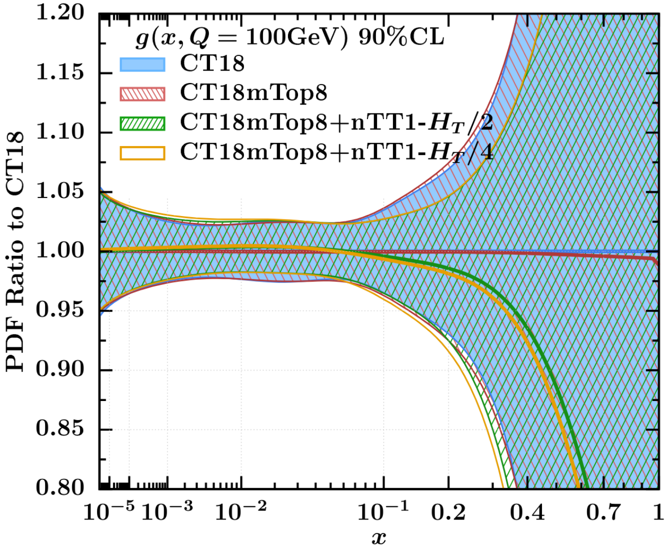

Global fit without jet and $t\bar{t}$ data vs CT18NNLO

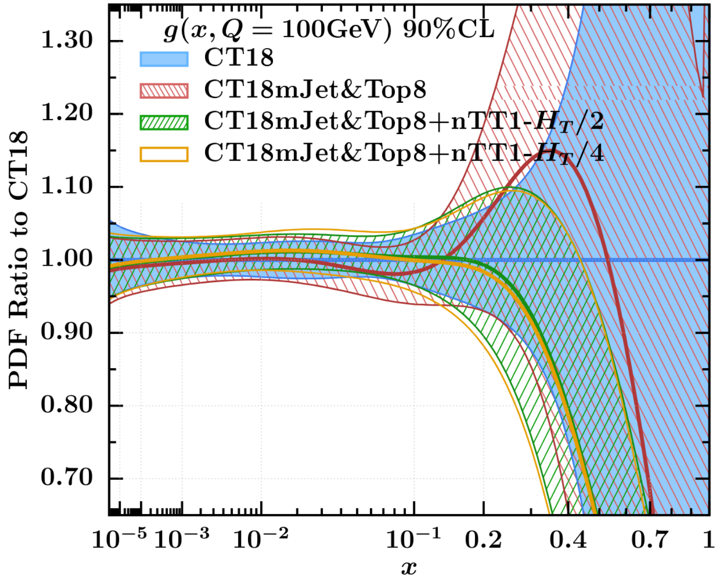

Tension

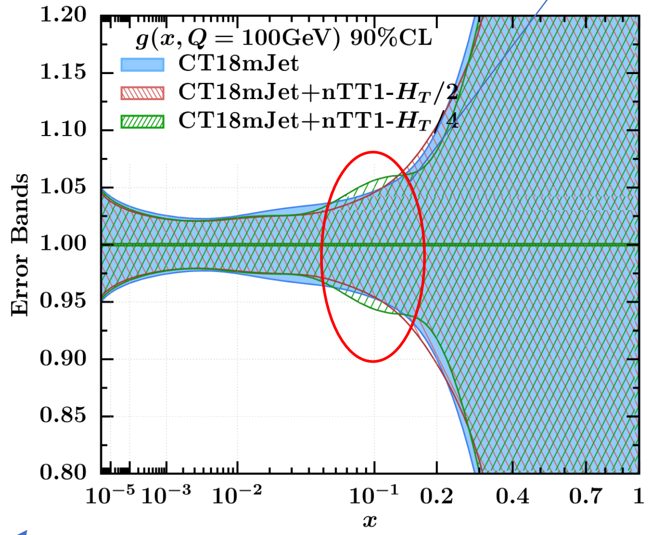

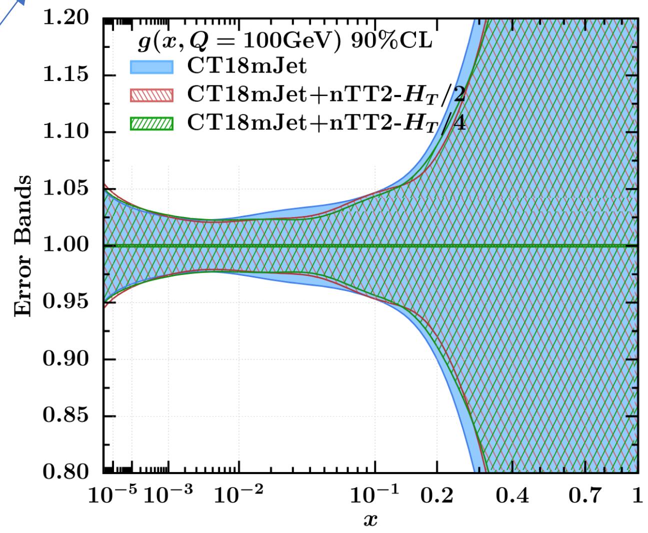

Differences between two optimal baseline selections of 13 TeV $t\bar{t}$ data

Theory errors: scale vs PDFs

Scale uncertainty: the recommended scale choice is not always the best. We select the scale choice that yields the smaller χ^2/Npt

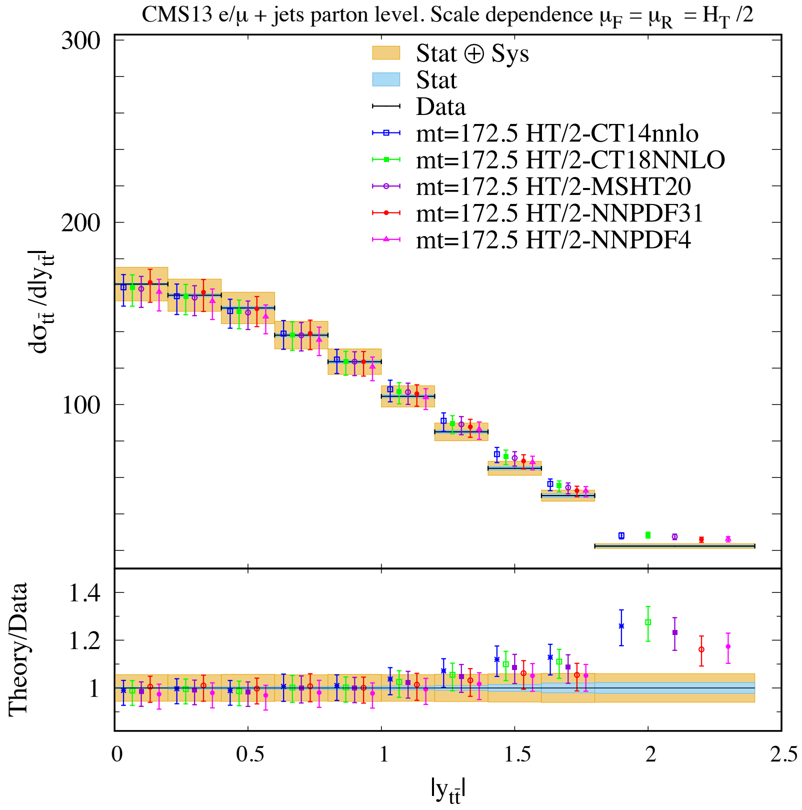

HT/2 varied up and down by a factor of 2

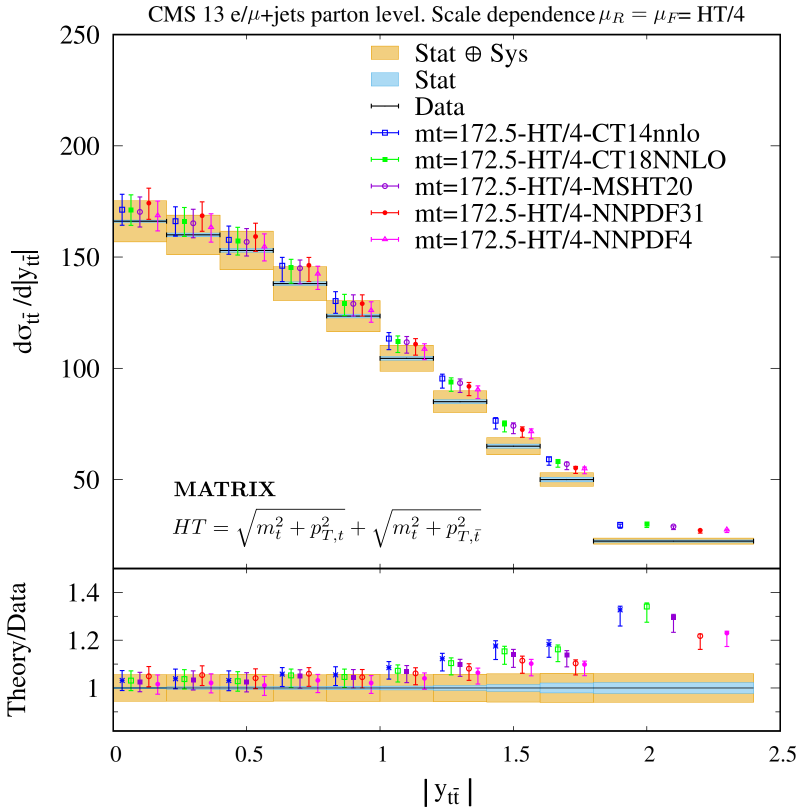

HT/4 varied up and down by a factor of 2

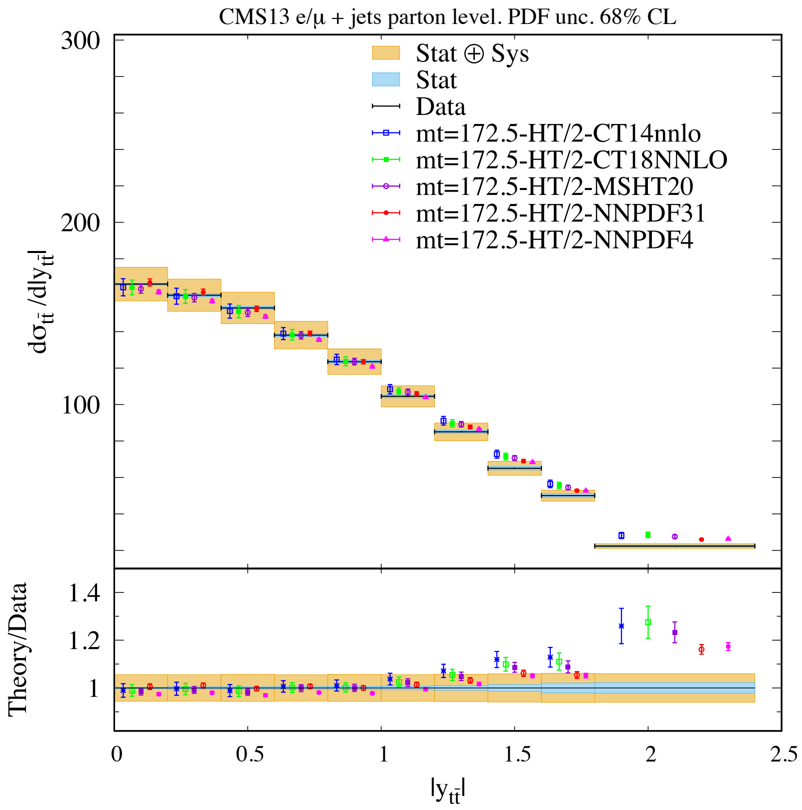

PDF Uncertainty @68% CL

Scale uncertainty comparable or larger than PDF uncertainty

Top-quark cross sections and distributions at aN^3LO

Theory calculation from Kidonakis 1405.7046, PRD (2014) and 1411.2633, PRD (2015) (Kidonakis, MG, Tonero, 2306.06166, PRD 2023)

$$d\sigma_{pp\to t\bar{t}} = \sum_{a,b} \int dx_a\, dx_b\, \phi_{a/p}(x_a,\mu_F)\, \phi_{b/p}(x_b,\mu_F)\, d\hat{\sigma}_{ab\to t\bar{t}}(s_4,\mu_F)$$

Laplace transf.

$$d\tilde{\sigma}_{ab\to t\bar{t}}(N) = \tilde{\phi}_{a/a}(N_a,\mu_F)\, \tilde{\phi}_{b/b}(N_b,\mu_F)\, d\tilde{\hat{\sigma}}_{ab\to t\bar{t}}(N,\mu_F)$$

$\tilde{\phi}(N) = \int_0^1 e^{-N(1-x)} \phi(x)\, dx$ and $d\tilde{\hat{\sigma}}_{ab\to t\bar{t}}(N) = \int_0^s (ds_4/s)\, e^{-Ns_4/s}\, d\hat{\sigma}_{ab\to t\bar{t}}(s_4)$

$$d\tilde{\sigma}_{ab\to t\bar{t}}(N) = \tilde{\psi}_{a/a}(N_a,\mu_F)\, \tilde{\psi}_{b/b}(N_b,\mu_F)\, \mathrm{tr}\left\{H_{ab\to t\bar{t}}\left(\alpha_s(\mu_R)\right)\, \tilde{S}_{ab\to t\bar{t}}\left(\frac{\sqrt{s}}{N\mu_F}\right)\right\}$$

Refactorization in the N-space

And from previous expressions

$$d\tilde{\hat{\sigma}}_{ab\to t\bar{t}}(N,\mu_F) = \frac{\tilde{\psi}_{a/a}(N_a,\mu_F)\, \tilde{\psi}_{b/b}(N_b,\mu_F)}{\tilde{\phi}_{a/a}(N_a,\mu_F)\, \tilde{\phi}_{b/b}(N_b,\mu_F)}\, \mathrm{tr}\left\{H_{ab\to t\bar{t}}\left(\alpha_s(\mu_R)\right)\, \tilde{S}_{ab\to t\bar{t}}\left(\frac{\sqrt{s}}{N\mu_F}\right)\right\}$$

Top-quark cross sections and distributions at aN^3LO

$$d\tilde{\hat{\sigma}}^{\rm resum}_{ab\to t\bar{t}}(N,\mu_F) = \exp\left[\sum_{i=a,b} E_i(N_i)\right] \exp\left[\sum_{i=a,b} 2\int_{\mu_F}^{\sqrt{s}} \frac{d\mu}{\mu}\gamma_{i/i}(N_i)\right] \times {\rm tr}\left\{H_{ab\to t\bar{t}}\left(\alpha_s(\sqrt{s})\right) \bar{P}\exp\left[\int_{\sqrt{s}}^{\sqrt{s}/N}\frac{d\mu}{\mu}\Gamma^\dagger_{S\,ab\to t\bar{t}}(\alpha_s(\mu))\right]\right.$$
$$\left. \times \tilde{S}_{ab\to t\bar{t}}\left(\alpha_s\left(\frac{\sqrt{s}}{N}\right)\right) P\exp\left[\int_{\sqrt{s}}^{\sqrt{s}/N}\frac{d\mu}{\mu}\Gamma_{S\,ab\to t\bar{t}}(\alpha_s(\mu))\right]\right\}$$

The inverse transform at fixed perturbative order, the soft-gluon corrections take the form of plus distributions of logs of s4

$$\frac{d^2\sigma^{(3)}_{ij\to t\bar{t}}}{dt_1\,du_1} = \left(\frac{\alpha_s}{\pi}\right)^5 \left\{D^{(5)}_{ij}\left[\frac{\ln^5(s_4/m_t^2)}{s_4}\right]_+ + D^{(4)}_{ij}\left[\frac{\ln^4(s_4/m_t^2)}{s_4}\right]_+ + D^{(3)}_{ij}\left[\frac{\ln^3(s_4/m_t^2)}{s_4}\right]_+\right.$$
$$\left. + D^{(2)}_{ij}\left[\frac{\ln^2(s_4/m_t^2)}{s_4}\right]_+ + D^{(1)}_{ij}\left[\frac{\ln(s_4/m_t^2)}{s_4}\right]_+ + D^{(0)}_{ij}\left[\frac{1}{s_4}\right]_+ + R_3\delta(s_4)\right\} + \ldots$$

which is matched to the fixed order NNLO calculation.

$t\bar{t}$ total cross section at aN^3LO

Kidonakis, MG, Tonero, 2306.06166, PRD 2023

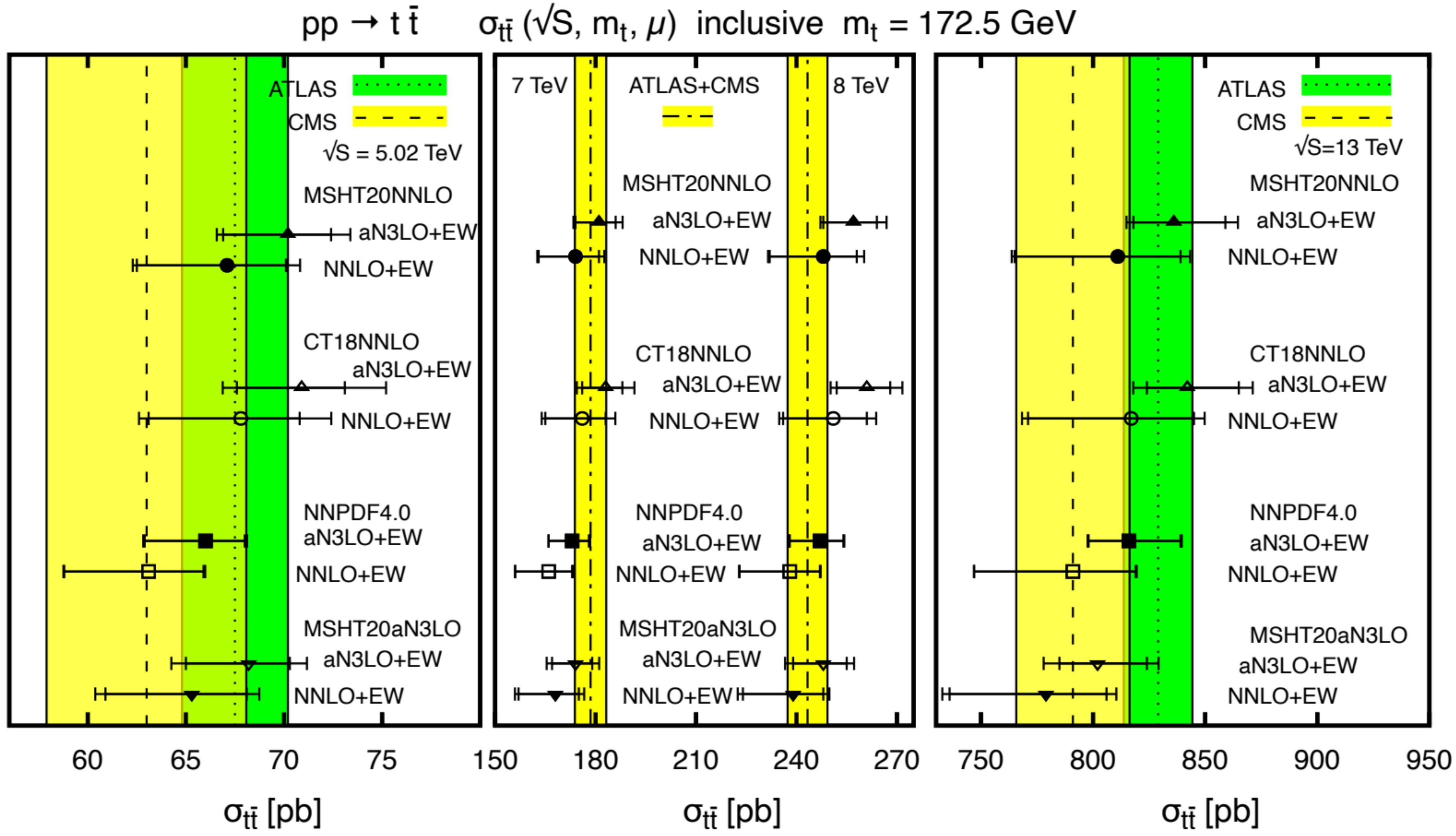

Theory error bars represent scale uncertainty (inner bar), and scale + pdf uncertainties in quadrature (outer bar).

The results at NNLO QCD are calculated using Top++2.0 (Czakon and Mitov CPC (2014)).
NLO QCD+EW -> MadGraph5 aMC@NLO (Alwall, et al. JHEP(2014); Frederix, Frixione, et al. JHEP (2018))

$t\bar{t}$ total cross section at aN^3LO

Kidonakis, MG, Tonero, 2306.06166, PRD 2023

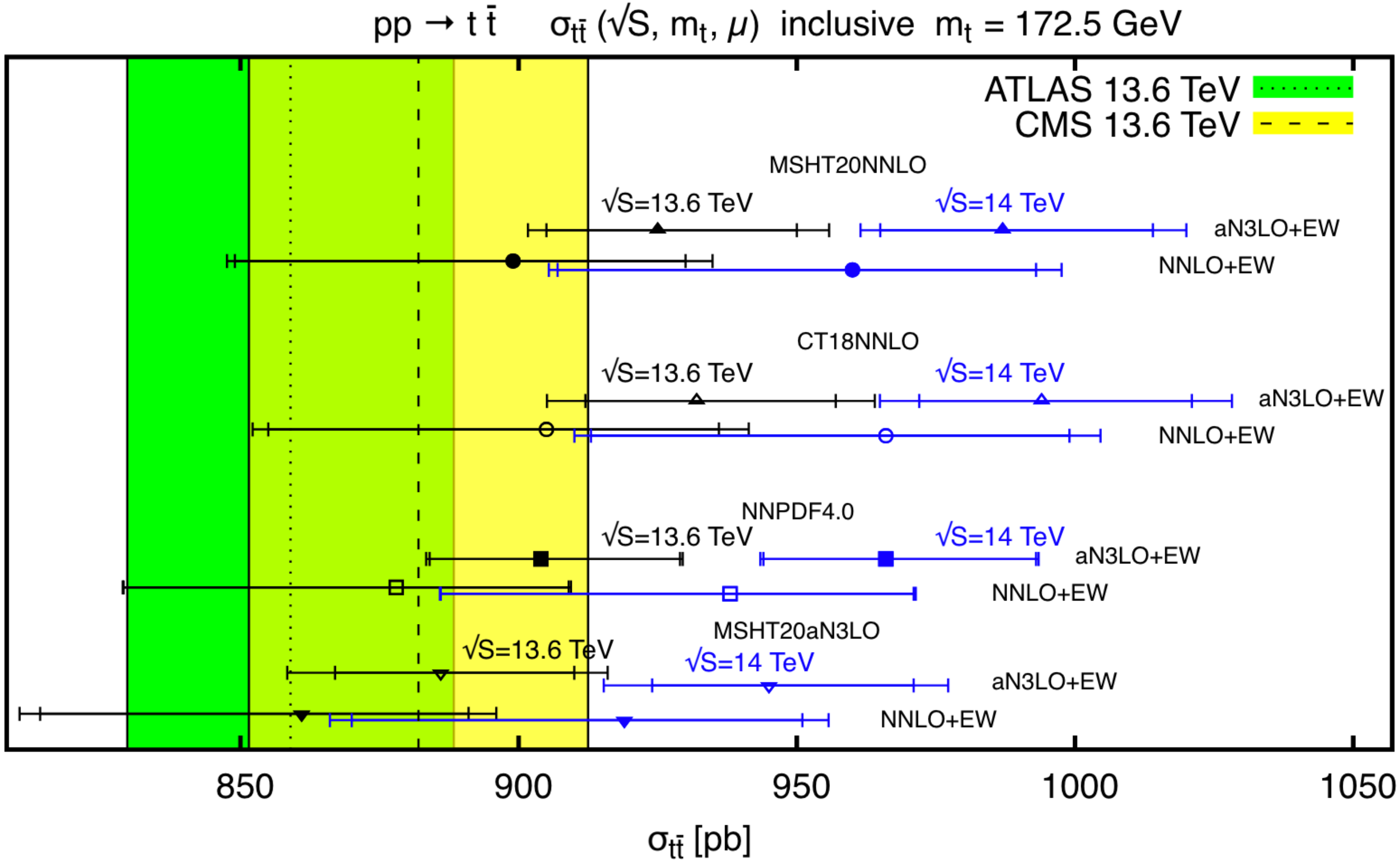

Theory error bars represent scale uncertainty (inner bar), and scale + pdf uncertainties in quadrature (outer bar).

The results at NNLO QCD are calculated using Top++2.0 (Czakon and Mitov CPC (2014)).
NLO QCD+EW -> MadGraph5 aMC@NLO (Alwall, et al. JHEP(2014); Frederix, Frixione, et al. JHEP (2018))

$t\bar{t}$ production at aN^3LO: top pT-distributions

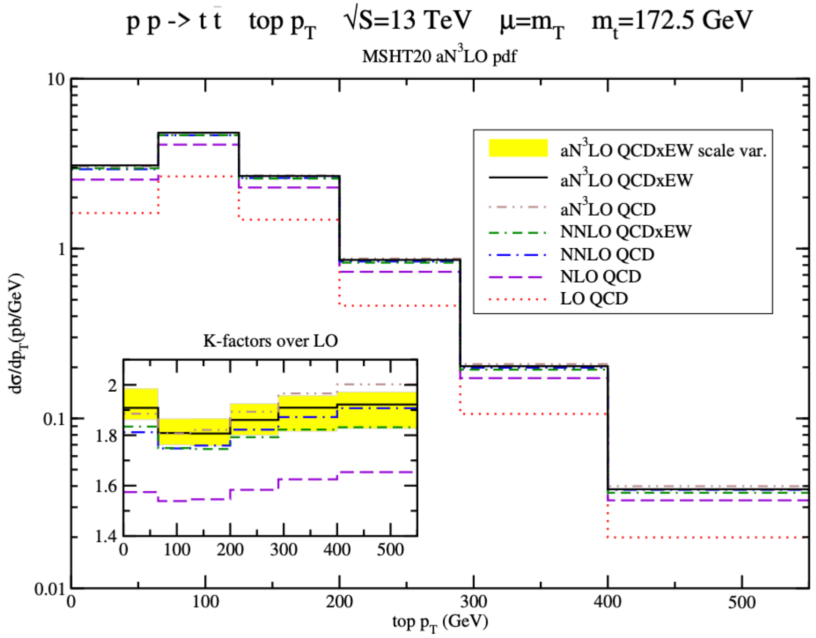

Kidonakis, MG, Tonero, 2306.06166, PRD 2023

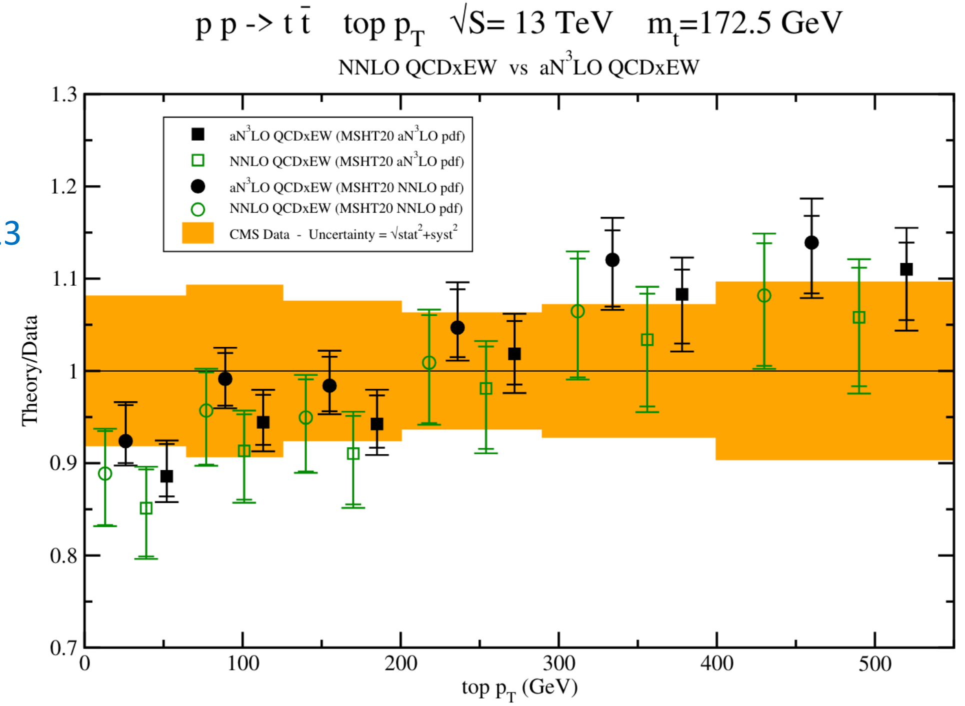

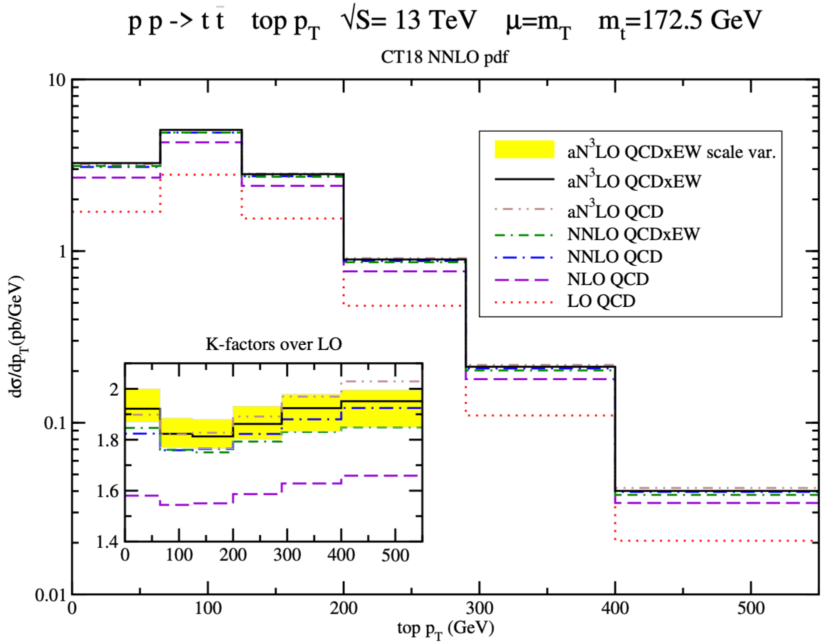

NLO EW corrections from Czakon, Heymes, et al. JHEP (2017) 1705.04105.

The combined QCDxEW corrections include $\mathcal{O}(\alpha_s^2\alpha)$ and the subleading $\mathcal{O}(\alpha_s\alpha^2)$, $\mathcal{O}(\alpha^3)$, $\mathcal{O}(\alpha_s^3\alpha)$ which are included using the multiplicative method discussed in 1705.04105

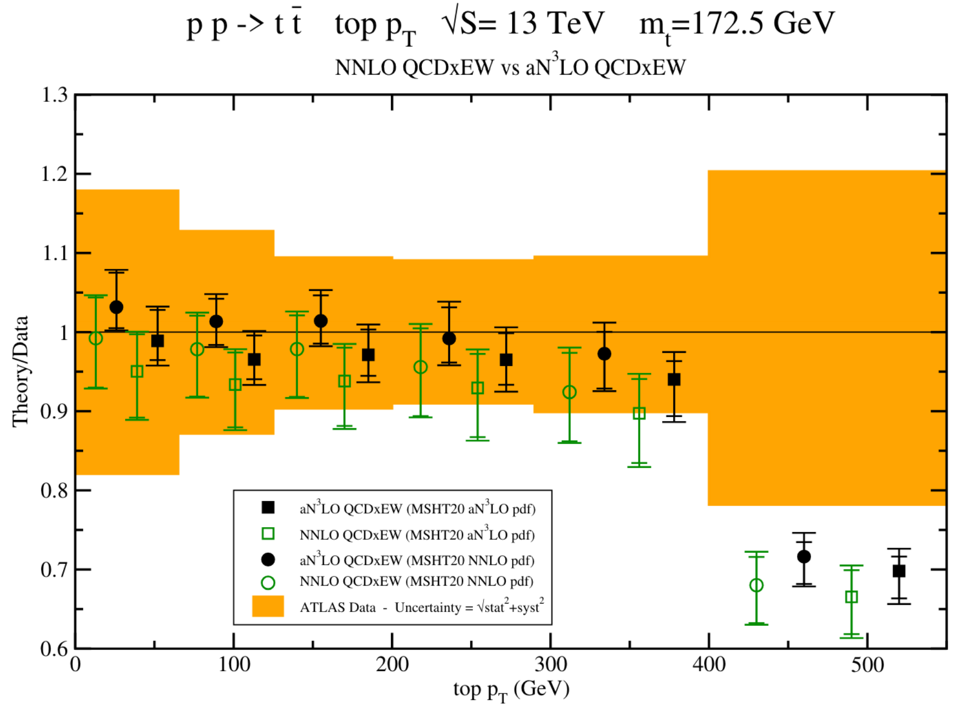

$t\bar{t}$ production at aN^3LO: top Y-distributions

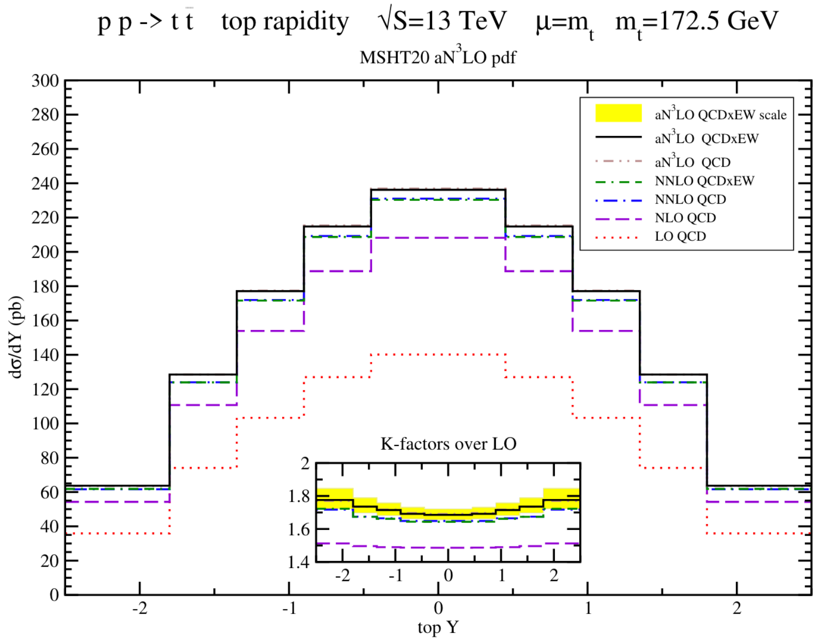

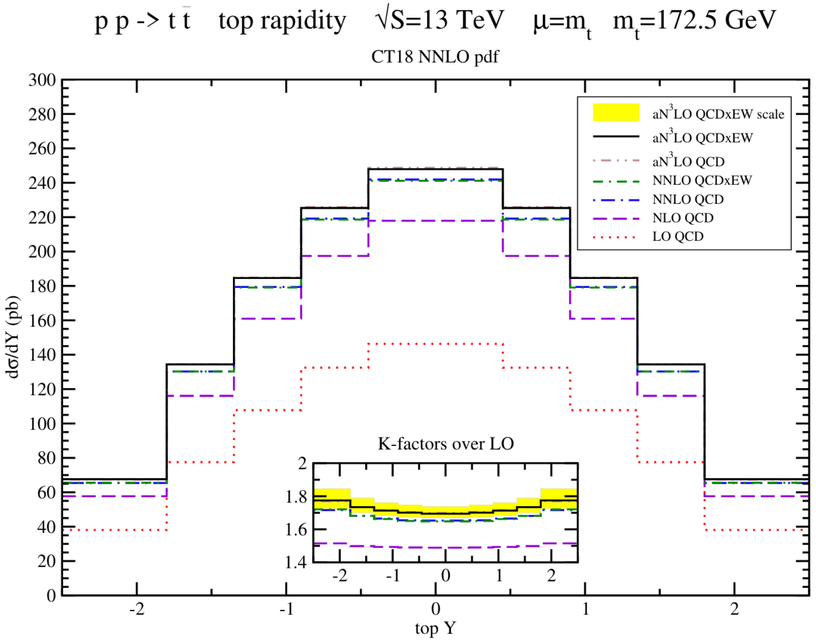

Kidonakis, MG, Tonero, 2306.06166, PRD 2023

NLO EW corrections from Czakon, Heymes, et al. JHEP (2017) 1705.04105.

The combined QCDxEW corrections include $\mathcal{O}(\alpha_s^2\alpha)$ and the subleading $\mathcal{O}(\alpha_s\alpha^2)$, $\mathcal{O}(\alpha^3)$, $\mathcal{O}(\alpha_s^3\alpha)$ which are included using the multiplicative method discussed in 1705.04105

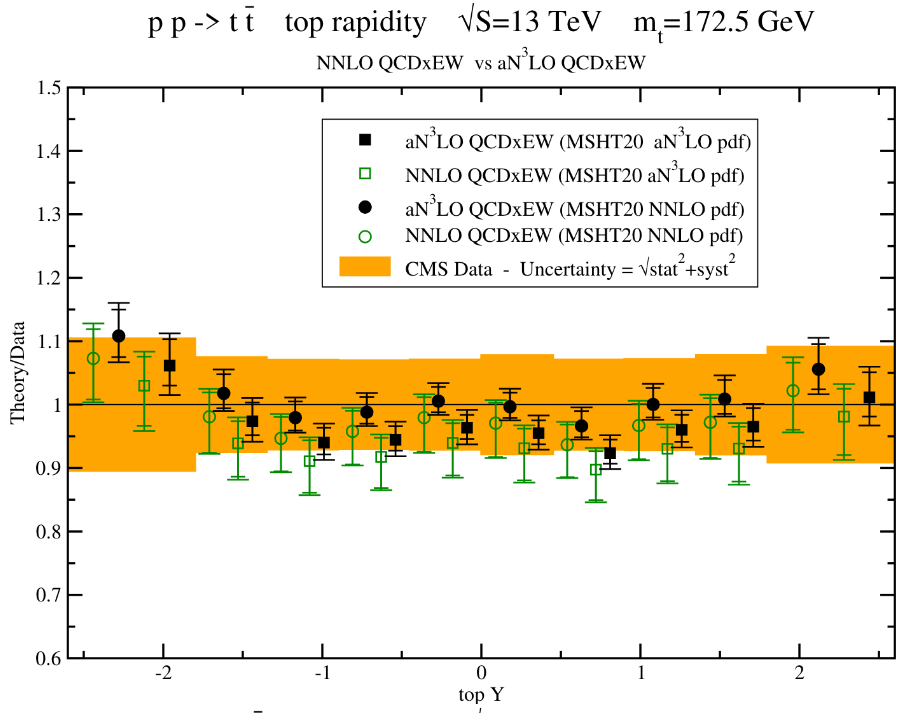

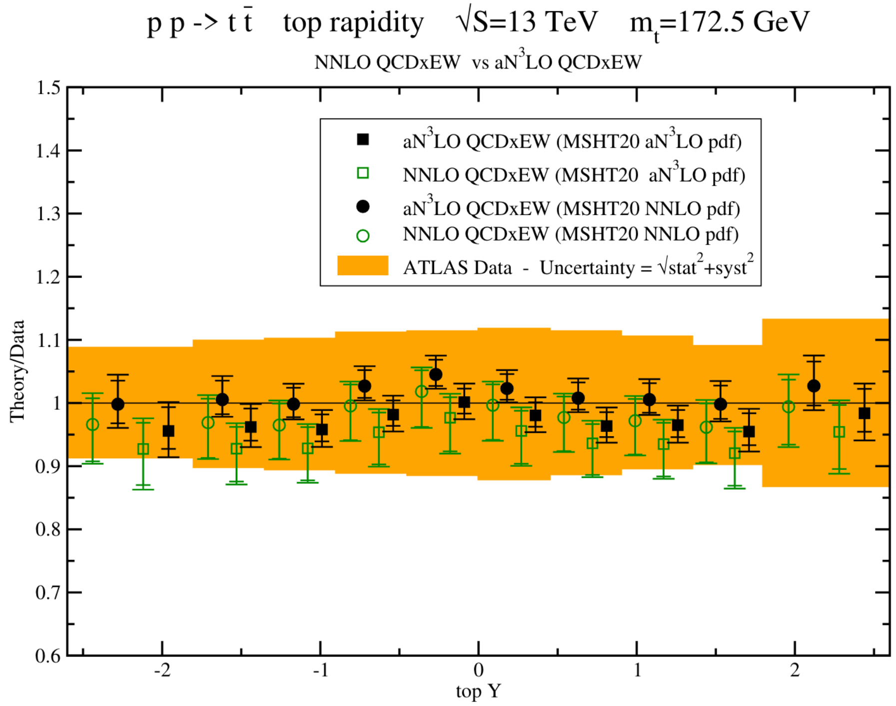

Summary

- First comprehensive study on the impact of LHC 13TeV $t\bar{t}$ data on CT PDFs
- Identified two optimal data selections: both have mild impact.
- Interplay between jets and $t\bar{t}$: jets still place stronger constraints on g(x)
- $t\bar{t}$ 13 TeV data prefer a softer gluon at large x, similar to the LHC jet data.
- Explored the impact of radiative corrections beyond NNLO using soft gluon resummation for the $t\bar{t}$ Xsec and 1D distributions theory.
- Explored the impact of EW corrections as well.
- QCD Corrections substantially increase the rates for $\sigma_{t\bar{t}}$, pT,t and Yt
- EW corrections important at large pT,t

BACK UP

The CT18 analysis

PHYSICAL REVIEW D **103**, 014013 (2021)

Editors' Suggestion

New CTEQ global analysis of quantum chromodynamics with high-precision data from the LHC

Tie-Jun Hou,[1,†] Jun Gao,[2] T. J. Hobbs,[3,4] Keping Xie,[3,5] Sayipjamal Dulat,[6,‡] Marco Guzzi,[7] Joey Huston,[8] Pavel Nadolsky,[3,§] Jon Pumplin,[8,*] Carl Schmidt,[8] Ibrahim Sitiwaldi,[6] Daniel Stump,[8] and C.-P. Yuan[8,∥]

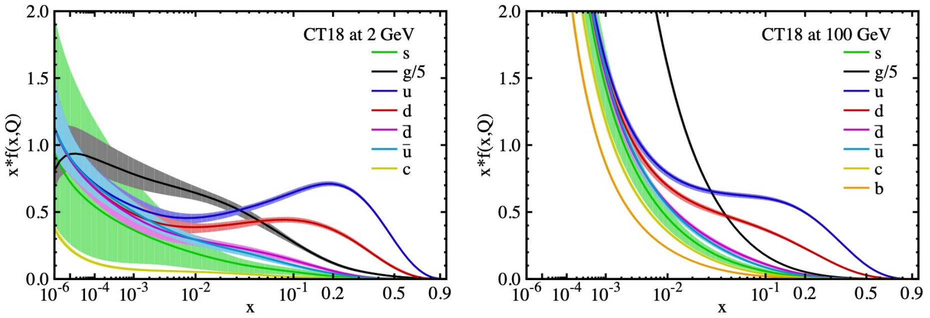

TABLE I. Datasets included in the CT18(Z) NNLO global analyses. Here we directly compare the quality of fit found for CT18 NNLO vs CT18Z NNLO on the basis of χ_E^2, $\chi_E^2/N_{pt,E}$, and S_E, in which $N_{pt,E}$, χ_E^2 are the number of points and value of χ^2 for experiment E at the global minimum. S_E is the effective Gaussian parameter [38,42,56] quantifying agreement with each experiment. The ATLAS 7 TeV 35 pb^{-1} W/Z dataset, marked by ‡‡, is replaced by the updated one (4.6 fb^{-1}) in the CT18A and CT18Z fits. The CDHSW data, labeled by †, are not included in the CT18Z fit. The numbers in parentheses are for the CT18Z NNLO fit.

Exp. ID#	Experimental dataset		$N_{pt,E}$	χ_E^2	$\chi_E^2/N_{pt,E}$	S_E
160	HERAI + II 1 fb^{-1}, H1 and ZEUS NC and CC $e^{\pm}p$ reduced cross sec. comb.	[30]	1120	1408 (1378)	1.3 (1.2)	5.7 (5.1)
101	BCDMS F_2^p	[57]	337	374 (384)	1.1 (1.1)	1.4 (1.8)
102	BCDMS F_2^d	[58]	250	280 (287)	1.1 (1.1)	1.3 (1.6)
104	NMC F_2^d/F_2^p	[59]	123	126 (116)	1.0 (0.9)	0.2 (−0.4)
108†	CDHSW F_2^p	[60]	85	85.6 (86.8)	1.0 (1.0)	0.1 (0.2)
109†	CDHSW $x_B F_3^p$	[60]	96	86.5 (85.6)	0.9 (0.9)	−0.7 (−0.7)
110	CCFR F_2^p	[61]	69	78.8 (76.0)	1.1 (1.1)	0.9 (0.6)
111	CCFR $x_B F_3^p$	[62]	86	33.8 (31.4)	0.4 (0.4)	−5.2 (−5.6)
124	NuTeV $\nu\mu\mu$ SIDIS	[63]	38	18.5 (30.3)	0.5 (0.8)	−2.7 (−0.9)
125	NuTeV $\bar{\nu}\mu\mu$ SIDIS	[63]	33	38.5 (56.7)	1.2 (1.7)	0.7 (2.5)
126	CCFR $\nu\mu\mu$ SIDIS	[64]	40	29.9 (35.0)	0.7 (0.9)	−1.1 (−0.5)
127	CCFR $\bar{\nu}\mu\mu$ SIDIS	[64]	38	19.8 (18.7)	0.5 (0.5)	−2.5 (−2.7)
145	H1 σ_r^b	[65]	10	6.8 (7.0)	0.7 (0.7)	−0.6 (−0.6)
147	Combined HERA charm production	[66]	47	58.3 (56.4)	1.2 (1.2)	1.1 (1.0)
169	H1 F_L	[33]	9	17.0 (15.4)	1.9 (1.7)	1.7 (1.4)
201	E605 Drell-Yan process	[67]	119	103.4 (102.4)	0.9 (0.9)	−1.0 (−1.1)
203	E866 Drell-Yan process $\sigma_{pd}/(2\sigma_{pp})$	[68]	15	16.1 (17.9)	1.1 (1.2)	0.3 (0.6)
204	E866 Drell-Yan process $Q^3 d^2\sigma_{pp}/(dQ dx_F)$	[69]	184	244 (240)	1.3 (1.3)	2.9 (2.7)
225	CDF run-1 lepton A_{ch}, $p_{T\ell} > 25$ GeV	[70]	11	9.0 (9.3)	0.8 (0.8)	−0.3 (−0.2)
227	CDF run-2 electron A_{ch}, $p_{T\ell} > 25$ GeV	[71]	11	13.5 (13.4)	1.2 (1.2)	0.6 (0.6)
234	DØ run-2 muon A_{ch}, $p_{T\ell} > 20$ GeV	[72]	9	9.1 (9.0)	1.0 (1.0)	0.2 (0.1)
260	DØ run-2 Z rapidity	[73]	28	16.9 (18.7)	0.6 (0.7)	−1.7 (−1.3)
261	CDF run-2 Z rapidity	[74]	29	48.7 (61.1)	1.7 (2.1)	2.2 (3.3)
266	CMS 7 TeV 4.7 fb^{-1}, muon A_{ch}, $p_{T\ell} > 35$ GeV	[75]	11	7.9 (12.2)	0.7 (1.1)	−0.6 (0.4)
267	CMS 7 TeV 840 pb^{-1}, electron A_{ch}, $p_{T\ell} > 35$ GeV	[76]	11	4.6 (5.5)	0.4 (0.5)	−1.6 (−1.3)
268‡‡	ATLAS 7 TeV 35 pb^{-1} W/Z cross sec., A_{ch}	[77]	41	44.4 (50.6)	1.1 (1.2)	0.4 (1.1)
281	DØ run-2 9.7 fb^{-1} electron A_{ch}, $p_{T\ell} > 25$ GeV	[78]	13	22.8 (20.5)	1.8 (1.6)	1.7 (1.4)
504	CDF run-2 inclusive jet production	[79]	72	122 (117)	1.7 (1.6)	3.5 (3.2)
514	DØ run-2 inclusive jet production	[80]	110	113.8 (115.2)	1.0 (1.0)	0.3 (0.4)

TABLE II. Like Table I, for newly included LHC measurements. The ATLAS 7 TeV W/Z data (4.6 fb^{-1}), labeled by ‡, are included in the CT18A and CT18Z global fits, but not in CT18 and CT18X.

Exp. ID#	Experimental dataset		$N_{pt,E}$	χ_E^2	$\chi_E^2/N_{pt,E}$	S_E
245	LHCb 7 TeV 1.0 fb^{-1} W/Z forward rapidity cross sec.	[81]	33	53.8 (39.9)	1.6 (1.2)	2.2 (0.9)
246	LHCb 8 TeV 2.0 fb^{-1} $Z \to e^-e^+$ forward rapidity cross sec.	[82]	17	17.7 (18.0)	1.0 (1.1)	0.2 (0.3)
248‡	ATLAS 7 TeV 4.6 fb^{-1}, W/Z combined cross sec.	[39]	34	287.3 (88.7)	8.4 (2.6)	13.7 (4.8)
249	CMS 8 TeV 18.8 fb^{-1} muon charge asymmetry A_{ch}	[83]	11	11.4 (12.1)	1.0 (1.1)	0.2 (0.4)
250	LHCb 8 TeV 2.0 fb^{-1} W/Z cross sec.	[84]	34	73.7 (59.4)	2.1 (1.7)	3.7 (2.6)
253	ATLAS 8 TeV 20.3 fb^{-1}, Z p_T cross sec.	[85]	27	30.2 (28.3)	1.1 (1.0)	0.5 (0.3)
542	CMS 7 TeV 5 fb^{-1}, single incl. jet cross sec., $R = 0.7$ (extended in y)	[86]	158	194.7 (188.6)	1.2 (1.2)	2.0 (1.7)
544	ATLAS 7 TeV 4.5 fb^{-1}, single incl. jet cross sec., $R = 0.6$	[9]	140	202.7 (203.0)	1.4 (1.5)	3.3 (3.4)
545	CMS 8 TeV 19.7 fb^{-1}, single incl. jet cross sec., $R = 0.7$, (extended in y)	[87]	185	210.3 (207.6)	1.1 (1.1)	1.3 (1.2)
573	CMS 8 TeV 19.7 fb^{-1}, $t\bar{t}$ norm. double-diff. top p_T and y cross sec.	[88]	16	18.9 (19.1)	1.2 (1.2)	0.6 (0.6)
580	ATLAS 8 TeV 20.3 fb^{-1}, $t\bar{t}$ p_T^t and $m_{t\bar{t}}$ abs. spectrum	[89]	15	9.4 (10.7)	0.6 (0.7)	−1.1 (−0.8)

Heavy-flavor production measurements at HERA and LHC included in the CT18 NNLO QCD global analysis.

Top-quark pair production diff. Xsec. measurements at 8TeV

What are data telling us?

- Heavy-quark production at the LHC at small p_T and large rapidity y of the heavy quark: sensitive to PDFs at both small and large x (especially true for c/b production)

$$x_{1,2} \approx \frac{\sqrt{p_T^2 + m_Q^2}}{\sqrt{S}} e^{\pm y}$$

- In this kinematic region PDFs are poorly constrained by other experiments in global PDF fits.
- Top-quark pair production @LHC can already probe the gluon PDF at $x \gtrsim 0.01$

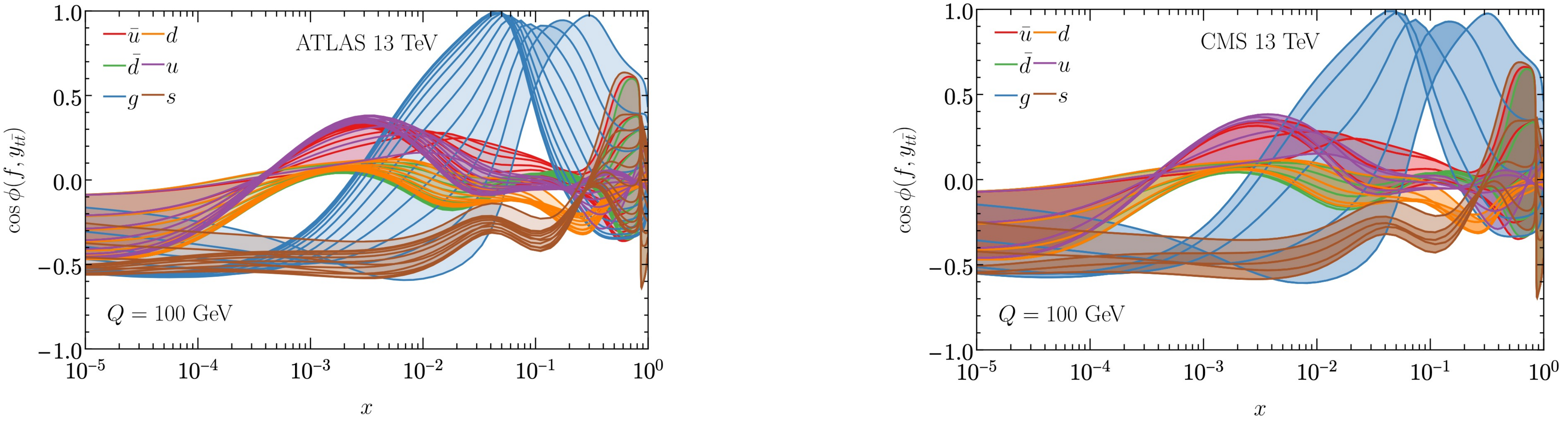

Correlation plots with ePump for the ATLAS all-hadronic and CMS dilepton channel data

PDF Kinematics in the Q-x plane

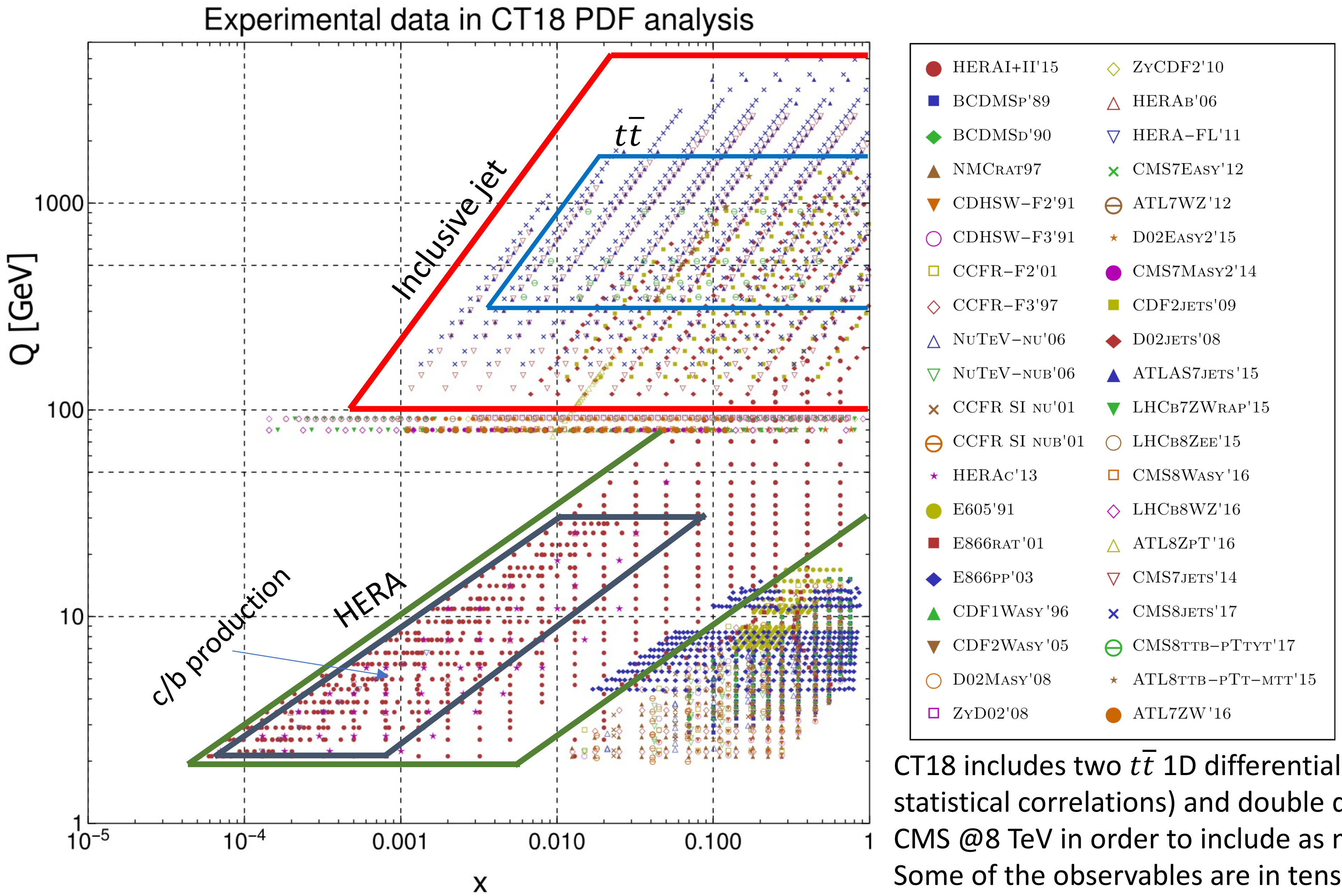

Jet and $t\bar{t}$ complement each other in the kinematic plane.
They impact the gluon PDF at large x. Important to disentangle the effect due to jet production and top-quark data.

Top and jet Data in CT18

Top-quark
1511.04716 ATLAS 8 TeV ttb ptT diff. distributions
1511.04716 ATLAS 8 TeV ttb mtt diff. distributions
1703.01630 CMS 8 TeV ttb (pT , yt) 2d diff. distrib.

Jet production
1406.0324 CMS incl. jet at 7 TeV with R=0.7
1410.8857 ATLAS incl. jet at 7 TeV with R=0.6
1609.05331 CMS incl. jet at 8 TeV with R=0.7

CT18 includes two $t\bar{t}$ 1D differential observables from ATLAS (using statistical correlations) and double differential measurements from CMS @8 TeV in order to include as much information as possible. Some of the observables are in tension with each other.

Numerical values for the $t\bar{t}$ total Xsec

$t\bar{t}$ total cross sections at LHC energies with MSHT20 NNLO pdf						
σ in pb	5.02 TeV	7 TeV	8 TeV	13 TeV	13.6 TeV	14 TeV
LO QCD	$40.9^{+15.5+1.2}_{-10.4-0.8}$	105^{+37+3}_{-25-2}	150^{+50+4}_{-35-2}	$487^{+142+10}_{-103-6}$	$540^{+155+10}_{-113-7}$	$576^{+163+11}_{-120-7}$
NLO QCD	$59.6^{+7.1+2.0}_{-8.1-1.2}$	155^{+19+4}_{-20-3}	222^{+26+6}_{-28-4}	730^{+85+14}_{-86-10}	809^{+94+16}_{-94-11}	$863^{+101+17}_{-99\ -11}$
NLO QCD+EW	$59.6^{+7.0+1.9}_{-8.1-1.2}$	155^{+18+4}_{-20-3}	221^{+26+6}_{-28-3}	727^{+83+14}_{-85-10}	806^{+92+15}_{-93-11}	860^{+99+17}_{-99-11}
NNLO QCD	$67.1^{+3.0+2.2}_{-4.6-1.4}$	$174^{+7\ +5}_{-11-3}$	249^{+10+7}_{-16-4}	814^{+28+16}_{-46-11}	902^{+31+18}_{-50-12}	963^{+33+18}_{-53-13}
NNLO QCD+EW	$67.1^{+3.0+2.2}_{-4.6-1.4}$	$174^{+7\ +5}_{-11-3}$	248^{+10+7}_{-16-4}	811^{+28+16}_{-46-11}	899^{+31+18}_{-50-12}	960^{+33+18}_{-53-13}
aN^{3}LO QCD	$70.2^{+2.2+2.3}_{-3.3-1.5}$	181^{+5+5}_{-7-3}	258^{+7+7}_{-9-4}	839^{+23+17}_{-18-11}	928^{+25+18}_{-20-12}	990^{+27+19}_{-22-13}
aN^{3}LO QCD+EW	$70.2^{+2.2+2.3}_{-3.3-1.5}$	181^{+5+5}_{-7-3}	257^{+7+7}_{-9-4}	836^{+23+17}_{-18-11}	925^{+25+18}_{-20-12}	987^{+27+19}_{-22-13}

$t\bar{t}$ total cross sections at LHC energies with MSHT20 aN^{3}LO pdf						
σ in pb	5.02 TeV	7 TeV	8 TeV	13 TeV	13.6 TeV	14 TeV
LO QCD	$40.0^{+14.9+1.1}_{-10.1-1.2}$	103^{+35+3}_{-24-3}	146^{+48+3}_{-34-4}	$469^{+133+9}_{-97\ -10}$	$518^{+145+10}_{-106-11}$	$553^{+153+11}_{-113-11}$
NLO QCD	$58.1^{+6.8+1.8}_{-7.8-2.0}$	151^{+17+4}_{-20-5}	215^{+25+5}_{-27-6}	700^{+80+15}_{-80-15}	775^{+89+16}_{-88-16}	828^{+94+16}_{-94-18}
NLO QCD+EW	$58.1^{+6.6+1.8}_{-7.8-2.0}$	150^{+17+4}_{-19-4}	214^{+25+6}_{-26-6}	698^{+78+14}_{-80-16}	772^{+88+16}_{-87-16}	825^{+92+16}_{-93-18}
NNLO QCD	$65.3^{+2.8+2.0}_{-4.4-2.2}$	$169^{+7\ +5}_{-11-5}$	$240^{+9\ +6}_{-15-7}$	781^{+27+16}_{-43-17}	864^{+30+18}_{-47-19}	922^{+32+18}_{-49-20}
NNLO QCD+EW	$65.3^{+2.8+2.0}_{-4.4-2.2}$	$168^{+7\ +5}_{-11-5}$	$239^{+9\ +6}_{-15-7}$	779^{+27+16}_{-43-17}	861^{+30+18}_{-47-19}	919^{+32+18}_{-49-20}
aN^{3}LO QCD	$68.2^{+2.1+2.1}_{-3.2-2.3}$	175^{+5+5}_{-7-5}	249^{+7+6}_{-9-7}	804^{+22+16}_{-17-17}	889^{+24+18}_{-19-20}	948^{+26+19}_{-21-21}
aN^{3}LO QCD+EW	$68.2^{+2.1+2.1}_{-3.2-2.3}$	174^{+5+5}_{-7-5}	248^{+7+6}_{-9-7}	802^{+22+16}_{-17-17}	886^{+24+18}_{-19-20}	945^{+26+19}_{-21-21}

Numerical values for the top-pT distribution

Top-quark p_T distribution at 13 TeV with MSHT20 aN^{3}LO pdf			
$d\sigma/dp_T$ in pb/GeV	aN^{3}LO QCD	aN^{3}LO QCD×EW	aN^{3}LO QCD / NNLO QCD
$0 < p_T < 65$ GeV	$3.05^{+0.12+0.06}_{-0.07-0.06}$	$3.09^{+0.12+0.06}_{-0.08-0.06}$	1.041
$65 < p_T < 125$ GeV	$4.81^{+0.15+0.09}_{-0.13-0.10}$	$4.81^{+0.15+0.10}_{-0.12-0.10}$	1.034
$125 < p_T < 200$ GeV	$2.70^{+0.09+0.05}_{-0.08-0.07}$	$2.68^{+0.08+0.05}_{-0.08-0.07}$	1.035
$200 < p_T < 290$ GeV	$0.873^{+0.031+0.021}_{-0.028-0.023}$	$0.858^{+0.030+0.021}_{-0.028-0.022}$	1.039
$290 < p_T < 400$ GeV	$0.209^{+0.005+0.006}_{-0.010-0.006}$	$0.203^{+0.005+0.006}_{-0.010-0.006}$	1.050
$400 < p_T < 550$ GeV	$0.0399^{+0.0010+0.0012}_{-0.0020-0.0013}$	$0.0383^{+0.0010+0.0012}_{-0.0019-0.0013}$	1.050

Data description of top-pT distributions

pdf	NNLO QCD	NNLO QCD ×EW	aN^{3}LO QCD	aN^{3}LO QCD ×EW
MSHT20 NNLO	2.57	1.58	3.27	2.15
MSHT20 aN^{3}LO	2.76	1.80	3.42	2.20
CT18 NNLO	2.86	1.79	3.68	2.44
NNPDF4.0 NNLO	1.56	0.91	1.92	1.09

Table 9: Summary of the χ^2/N_{pt} for the top-quark p_T distributions at CMS.

pdf	NNLO QCD	NNLO QCD ×EW	aN^{3}LO QCD	aN^{3}LO QCD ×EW
MSHT20 NNLO	1.07	1.27	1.40	1.48
MSHT20 aN^{3}LO	1.05	1.22	1.42	1.43
CT18 NNLO	1.17	1.30	1.53	1.57
NNPDF4.0 NNLO	1.18	1.58	1.32	1.62

Table 10: Summary of the χ^2/N_{pt} for the top-quark p_T distributions at ATLAS.

Data description of top-Y distributions

pdf	NNLO QCD	NNLO QCD ×EW	aN^3LO QCD	aN^3LO QCD ×EW
MSHT20 NNLO	0.71	0.76	0.66	0.70
MSHT20 aN^3LO	0.85	0.91	0.79	0.83
CT18 NNLO	0.86	0.92	0.81	0.88
NNPDF4.0 NNLO	0.68	0.71	0.56	0.61

Table 15: Summary of the χ^2/N_{pt} for the top-quark rapidity distributions at CMS.

pdf	NNLO QCD	NNLO QCD ×EW	aN^3LO QCD	aN^3LO QCD ×EW
MSHT20 NNLO	0.70	0.66	0.49	0.44
MSHT20 aN^3LO	0.70	0.66	0.56	0.46
CT18 NNLO	0.71	0.69	0.71	0.70
NNPDF4.0 NNLO	1.26	1.18	0.90	0.84

Table 16: Summary of the χ^2/N_{pt} for the top-quark rapidity distributions at ATLAS.